J Membrane Biol
DOI 10.1007/s00232-016-9894-1

Lipid-Detergent Phase Transitions During Detergent-Mediated Liposome Solubilization

Hanieh Niroomand[1,2] · Guru A. Venkatesan[3] · Stephen A. Sarles[3] · Dibyendu Mukherjee[1,2,3] · Bamin Khomami[1,2,3]

Received: 29 October 2015 / Accepted: 24 March 2016

Abstract We investigate the phase transition stages for detergent-mediated liposome solubilization of bio-mimetic membranes with the motivation of integrating membrane-bound Photosystem I into bio-hybrid opto-electronic devices. To this end, the interaction of two non-ionic detergents *n-dodecyl*-β-D-maltoside (DDM) and Triton X-100 (TX-100) with two types of phospholipids, namely DPhPC (1,2-diphytanoyl-*sn*-glycero-3-phosphocholine) and DPPG (1,2-dipalmitoyl-*sn*-glycero-3-phospho-(1′-*rac*-glycerol)), are examined. Specifically, solubilization processes for large unilamellar liposomes are studied with the aid of turbidity measurements, dynamic light scattering, and cryo-transmission electron microscopy imaging. Our results indicate that the solubilization process is well depicted by a three-stage model, wherein the lamellar-to-micellar transitions for DPhPC liposomes are dictated by the critical detergent/phospholipid ratios. The solubilization of DPhPC by DDM is devoid of formation of a "gel-like" phase. Furthermore, our results indicate that DDM is a stable candidate for DPhPC solubilization and proteoliposome formation. Finally, although the solubilization of DPPG with DDM indicated the familiar three-stage process, the same process with TX-100 indicate structural deformation of vesicles into complex network of kinetically trapped micro- and nanostructured arrangements of lipid bilayers.

Keywords Detergent-mediated liposome solubilization · DPhPC and DPPG · *n-dodecyl*-β-D-maltoside (DDM) and Triton X-100 (TX-100) · Lamellar-to-micellar transition · Lamellar-to-complex structures · Transmission electron microscopy

Introduction

Membranes play a critical role in defining the structure and function of all prokaryotic and eukaryotic cells in plants and animals. Membranes define compartments, and their structures determine the nature of all communication between the inside and outside of cellular regions. Proteins and lipids constitute the major components of membranes. Phospholipids, either in the form of bimolecular leaflets or in micellar arrangements, constitute the foundations of membrane structure (Levine et al. 1968). The relative amount of proteins and lipids vary significantly, ranging from about 20 % (dry weight) protein (myelin) to 80 % protein (mitochondria) (Gennis 1989). A fundamental understanding of the solution phase morphologies during membrane-surfactant (detergent) interactions is critical for successful isolation, purification, reconstitution, and crystallization of membrane proteins (Silvius 1992; Rigaud et al. 1995; Pata et al. 2004; Lichtenberg et al. 1983; Kragh-Hansen et al. 1998; Lopez et al. 1999; Lopez et al. 2001). Such morphological characterization is also

Electronic supplementary material The online version of this article (doi:10.1007/s00232-016-9894-1) contains supplementary material, which is available to authorized users.

✉ Dibyendu Mukherjee
dmukherj@utk.edu

✉ Bamin Khomami
bkhomami@utk.edu

[1] Sustainable Energy Education and Research Center (SEERC), University of Tennessee, Knoxville, TN, USA

[2] Department of Chemical and Biomolecular Engineering, University of Tennessee, Knoxville, TN, USA

[3] Department of Mechanical, Aerospace and Biomedical Engineering, University of Tennessee, Knoxville, TN, USA

Published online: 12 April 2016

important for understanding the formation mechanism of complex structures by membrane proteins and detergents when reconstituted into artificial lipid membranes—a critical research area for the development of new drugs (Deamer and Bangham 1976; Helenius et al. 1979; Szoka and Papahadjopoulos 1980; Cladera et al. 1997; Paternostre et al. 1988).

The present study is motivated by the need for incorporation and assembly of individually oriented Photosystem I (PS I), a trimeric photosynthetic trans-membrane protein complex of relatively large size ($\sim$1000 kDa), into membrane-bound structures that mimic the natural thylakoid membrane housing of PS I. Such membrane-bound assembly of PS I complexes finds wide applications from membrane protein crystallization to our research interests in designing bio-hybrid opto-electronic devices. Specifically, the lipid content of a thylakoid membrane predominantly consists of two kinds of phospholipid, phosphatidylcholine (PC), and phosphatidylglycerol (PG), along with other glycolipids, such as monogalactosyl diacylglycerol (MGDG), digalactosyl diacylglycerol (DGDG), and sulfoquinovosyl diacylglycerol (SQDG) (Sato 2004; Douce et al. 1973; Mendiolamorgenthaler et al. 1985; Gombos et al. 1996).

To this end, we focus our attention on the potential use of PC and PG lipid membranes to mimic bilayer systems that provide bio-mimetic housing for PS I extracted from *Thermosynechococcus elongatus* (*T. elongatus*). Four basic strategies can be used for the insertion of membrane proteins into liposomes. These include sonication, freeze–thawing, organic solvents, and detergents. The first three methods have limitations in efficient proteoliposome reconstitution including possible local probe heating during sonication that leads to degradation and denaturation of many membrane proteins. Similarly, organic solvents denature most amphiphilic membrane proteins even though reverse-phase evaporation and solvent injection using organic solvents enable efficient liposome preparations (Deamer and Bangham 1976; Szoka and Papahadjopoulos 1980). However, since membrane protein purification regularly requires the use of detergents, detergent-mediated solubilization has become a preferred route for proteoliposome preparations (Rigaud and Levy 2003). Furthermore, our recent studies reveal that two prototypical nonionic detergents—*n-dodecyl*-β-D-maltoside (DDM) and Triton X-100 (TX-100)—with low critical micellar concentrations (CMC) can be systematically used for PS I solubilization without denaturing the protein (Mukherjee et al. 2010, 2011a, b).

Membrane solubilization typically comprises a three-stage process represented by the structural transitions that occur as detergents interact with lipid membranes (Silvius 1992; Lichtenberg 1983; Kragh-Hansen et al. 1998; Lichtenberg et al. 2000). These transitions are typically analyzed qualitatively by turbidity measurements (Rigaud and Levy 2003). As a function of increasing detergent concentrations, the abovementioned stages are as follows: (I) a stage containing detergent monomers and vesicles wherein detergent monomers start getting incorporated into vesicles; (II) a stage where detergent monomers, mixed vesicles and mixed micelles coexist (detergent being incorporated into vesicles); and (III) a stage that consists purely of micelles at varying detergent/lipid ratios and detergent monomers. In the first stage, detergent molecules incorporate into the lipid bilayer without disrupting the membrane, and the vesicle remains intact. This detergent insertion induces an initial swelling of the liposomes (Geertsma et al. 2008) that leads to the critical detergent concentration, R_{sat}, marking the onset of solubilization in typical optical density measurement data (shown by the cartoon in Fig. 1a). Further increase in detergent concentration yields higher detergent insertion (stage II), which causes some of the vesicles to break into lipid micelles that can coexist with detergent-saturated vesicles and detergent micelles. This process is linked with bilayer flip-flop (detergent flip over from outer monolayer into the inner monolayer of the bilayer) where, based on the choice of detergents and lipids, different mechanisms of membrane solubilizations can be initiated (Kragh-Hansen et al. 1998; Lichtenberg et al. 2013a). Typically, turbidity measurements show a decreasing trend during this stage up to the point marked as R_{sol}, where the optical density reaches its minimum, indicating a complete solubilization of liposomes by detergent molecules. Finally, all membrane components are fully solubilized into mixed micelles (stage III) once the detergent concentration in the bilayer exceeds R_{sol}, and the suspension becomes optically transparent (Lambert et al. 1998). It should be mentioned here that earlier works on detergent-mediated membrane protein reconstitution mostly report a window of detergent concentrations between the saturation and solubilization point as the suitable point for protein insertion. Yet, very little is known regarding the optimal morphology of the lipid-detergent mixed bilayer systems that promote the interfacial chemistry for membrane protein assembly.

Few prior studies have systematically investigated the detailed role of lipid-detergent interactions during detergent-mediated protein reconstitution in liposomes. In the past, most studies on the solubilization of phosphatidylcholine lipids with TX-100 (Lichtenberg 1983; Lichtenberg et al. 2013b) and DDM (Knol et al. 1998) involve PC lipids from egg, plant or *E. coli*. More recently, synthetic lipids are also used in lipid-detergent interaction studies (Arnulphi et al. 2007; Stuart and Boekema 2007; Sudbrack et al. 2011; Nazari et al. 2012; Heerklotz and Seelig 2000). In an effort to achieve lipid compositions that both mimic

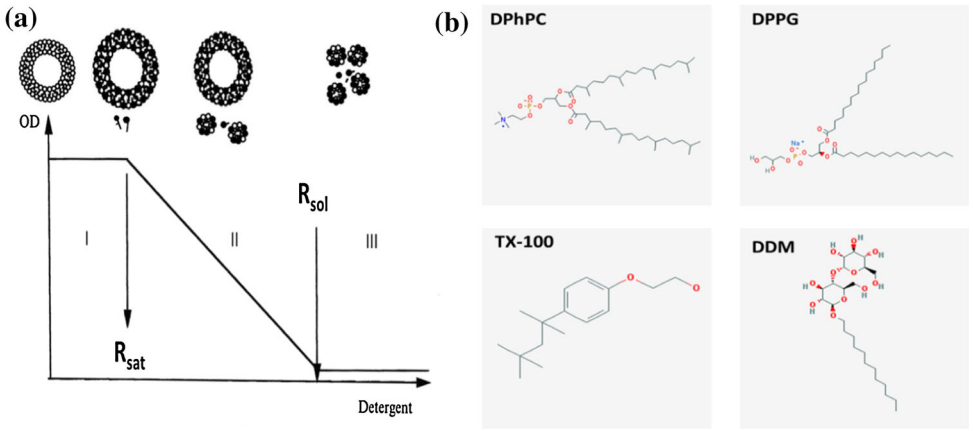

Fig. 1 **a** Graphical representation of different stages during the lamellar-to-micellar transition; **b** molecular structure of lipids (DPhPC, DPPG) and detergents (TX-100, DDM). DPhPC and DPPG are molecules with two hydrocarbon chains of 16 carbons with total lipid molecule length of ~2–3 nm. TX-100 molecule length is ~3.75–4.0 nm, and DDM molecule length is ~2.75–3.0 nm. Detergent molecule sizes given are based on half of the micellar hydrodynamic diameter (Mukherjee et al. 2011a)

natural thylakoid membrane systems and provide robust bio-mimetic housings for PS I, we study purely synthetic lipids with saturated fatty acids, which eliminate the complexity of natural phospholipids due to different acyl-chains. Past studies have mostly focused on detergent-mediated transport protein reconstitutions in liposomes prepared from PC plus phosphatidic acid (PA) with detergents such as TX-100, *n*-octyl β-D-glucopyranoside (octylglucoside), octaethylene glycol monododecyl ether (C12E8), sodium cholate, or sodium deoxycholate (Cladera et al. 1997; Rigaud et al. 1988). Similar studies with transport proteins have also been performed in liposomes prepared from *E. coli*, and *E. coli* plus egg PC with DDM and TX-100 as detergents (Geertsma et al. 2008; Knol et al. 1998; Gaillard et al. 1996). However, few studies have been conducted for small membrane proteins with molecular weights of ~30–80 kDa (Lévy et al. 1992; Coelfen et al. 1996; Hagting et al. 1997; Parmar et al. 1999). And, only a handful of attempts have been made to date to reconstitute large membrane proteins into liposomes. To this end, fluorescence quenching measurements have been used to monitor detergent-mediated incorporation of monomeric PS I reaction centers (extracted from *Synechocystis sp* PCC6803), in liposomes prepared from egg PC and PA lipids (Cladera et al. 1996). Protein activity has also been monitored for PS I particles from spinach incorporated into PG lipid complex (Yang et al. 2005), but both the aforementioned works lack imaging techniques. However, recent AFM measurements of three membrane proteins from the bacterial photosynthetic apparatus reconstituted into a planar lipid bilayer (Milhiet et al. 2006), leaving room for a clear elucidation of the structural and morphological arrangements in the proteoliposome formation.

To address these knowledge gaps, the first rational step requires systematic and detailed morphological characterizations of the phase transitions during detergent-mediated liposome solubilization. Specifically, we investigate the morphological variations induced by the detergent-mediated solubilization of 1,2-diphytanoyl-*sn*-glycero-3-phosphocholine (DPhPC) and 1,2-dipalmitoyl-*sn*-glycero-3-phospho-(1′-*rac*-glycerol) (DPPG) liposomes by the two non-ionic detergents, DDM, and TX-100 by means of turbidity measurements, dynamic light scattering, negative staining electron microscopy (NS-EM), and cryo-transmission electron microscopy (cryo-TEM). Each of the aforementioned measurements is systematically conducted during different stages of stepwise solubilization of preformed liposomes with varying detergent concentrations.

For ease of visualization and understanding, Fig. 1b represents the structural details of lipids (DPhPC and DPPG) and detergents (DDM and TX-100). Because of their branched hydrophobic side chains (as shown in Fig. 1b earlier), DPhPC membranes exhibit greater mechanical stability and lower permeation to ions and water than unbranched phospholipids (Baba et al. 1999). While not native to plants or animals, DPhPC has been a good choice of phospholipid for the study of reconstituted channel-forming proteins (Koeppe and Andersen 1996; Spassova et al. 1995), crystallization of proton channel peptides (Lovejoy et al. 1992), and ion-conducting measurements (Hsieh et al. 1997). Other forms of artificial lipid membranes such as black lipid membranes (BLMs), supported lipid membranes (SLBs), giant unilamellar vesicles (GUVs), and droplet interface bilayers (DIBs) have also utilized DPhPC to form highly stable membrane models (Sokolov et al. 2007; Andersson et al. 2011; Bayley et al. 2008). In addition, the methylated side chains of DPhPC

enable it to exhibit high chemical stability over a wide pH range and cause it to exist in a fluid-like thermotropic state across a wide temperature range (at least from −20 to 70 °C) without any detectable gel-to-liquid crystalline phase transition, perhaps owning to steric interference of the methyl groups in the ordered packing of the isoprenoid residues (Andersson et al. 2011; Lindsey et al. 1979). On the other hand, DPPG is an anionic phospholipid with gel-to-liquid crystalline transition temperature at ∼41 °C and devoid of any methyl branches (see Fig. 1b earlier) (Morrow et al. 2007). DPPG is frequently used as mimetics of bacterial membranes in biophysical studies on the effect of antimicrobial peptides (Konovalov et al. 2002; Lohner et al. 2001).

The results presented in this work shed light to the suitability of DDM or TX-100 as the detergent of choice for the solubilization of both DPhPC and DPPG lipids. Our observations indicate that, depending on the detergents (DDM or TX-100) and the lipids (DPhPC and DPPG) used, two possible pathways can result in the well-known, three-stage solubilization process or a phase transition into networks of complex structural arrangements. The present study uses the aforementioned characterizations to reveal the mechanism by which membrane bilayers undergo complex structural arrangements during different stages of their solubilization process. In turn, such studies pave the path for determining the specific morphological arrangements of lipid bilayer membranes constructed from DPhPC and DPPG that are suitable for detergent-mediated membrane protein reconstitution and successful PS I-proteoliposome formation.

Experimental Section

Materials

Dibasic (Na_2HPO_4) and monobasic (NaH_2PO_4) sodium phosphate with >99 % assay were purchased from Fisher Scientific to prepare the aqueous buffer solutions of 200 mM Na-Phosphate with pH = 7.0. All aqueous buffer solutions of 200 mM Na-Phosphate were prepared in ultrapure de-ionized (D.I.) water with a resistivity of 18.2 MΩ cm at 25 °C (Millipore, Billerica, MA). *n*-dodecyl-β-D-maltoside (DDM) was purchased from Gold Biotechnology, whereas Triton X-100 (10 % w/v aqueous solution) was obtained from Anatrace. 1,2-diphytanoyl-*sn*-glycero-3-phosphocholine (DPhPC) and 1,2-dipalmitoyl-*sn*-glycero-3-phospho-(1′-*rac*-glycerol) (DPPG) were purchased as lyophilized powders from Avanti Polar Lipids, Inc. Polycarbonate filters were also purchased from Avanti Polar Lipids, Inc. Phosphotungstic acid hydrate (PTA) was purchased from electron microscopy sciences. Potassium hydroxide pellets (KOH) with >99 % assay were purchased from Fisher Scientific. Carbon-coated (400 mesh) copper grids and lacy carbon-coated (200 mesh) copper grids were purchased from SPI supplies, USA.

Methods

Liposome Preparation

4 mg ml^{-1} lipid suspensions were prepared in 200 mM Na-Phosphate (pH = 7.0) buffer, followed by 3–4 freeze–thaw cycles to form multilamellar liposomes. These suspensions were then extruded through 100 nm pore sized filter using a mini-extruder (Avanti Polar Lipids) to form unilamellar vesicles at room temperature for DPhPC suspension and at 50 °C for DPPG (i.e., above the transition temperature of DPPG at 41 °C). The large unilamellar vesicle size of ∼100 nm was confirmed from dynamic light scattering measurements. Further details regarding the lipid vesicle preparations can be found in previous literatures (Lichtenberg and Barenholz 2006).

Titrations of Liposomes with Detergent

Liposomes suspensions of 4 mg ml^{-1} titrated by stepwise addition of several aliquots of 10 wt% vol^{-1} of TX-100 or DDM to 5 ml of the liposome suspension. Detailed technical specifications regarding the physical properties of DDM and TX-100 are provided in Table S1 of Supplementary Material (Helenius et al. 1979; Knol et al. 1998; Helenius and Simons 1975). The effect of detergent on the liposomes was monitored by measuring the optical density at 540 nm (optimal wavelength for liposome adsorption) with a hybrid multi-mode microplate reader (Make: Biotek; Model: Synergy H1). All turbidity data were averaged over four experimental runs.

Dynamic Light Scattering (DLS)

To analyze the liposome size alterations induced by the interaction with the detergent molecules, dynamic light scattering measurements were carried out using a 632.8 nm-wavelength Zetasizer (Malvern Instruments). All DLS data were collected using a 178° backward scattering and averaged over four experimental runs each of which were summed up over 12 time correlograms fitted by the Zetasizer software. Due to the presence of bimodal or multimodal size distributions in some phase stages of the solubilization process, the DLS data are represented by more than one curve. All reported sizes are in terms of equivalent spherical hydrodynamic radius as estimated from Stokes–Einstein relation, and all DLS analyses are represented in terms of number distribution or volume

distribution. The data analysis was carried out using the effective thermo-physical properties of 200 mM Na-Phosphate aqueous buffer solutions with pH = 7.0. Previous kinetic studies of the interactions of DDM with preformed liposomes indicate a delay time of ~2–3 h to achieve equilibration for constant light-scattering data. Hence, to ascertain complete detergent equilibration, DLS and turbidity measurement of DDM interactions with liposomes were performed 4 h after detergent-lipid suspension preparation.

Scanning Transmission Electron Microscopy (STEM)

Negative staining embeds and supports the thin layer of biological sample by a dried layer of heavy metal-containing salt, thereby increasing the contrast of biological material with their surroundings without causing structural alteration (De Carlo and Harris 2011; Hayat and Miller 1990). A sequential two-droplet method was used for negative staining. Aliquots (~5 µl) of the lipid/detergent in buffer suspensions were adhered to thin carbon-coated 400-mesh copper grids that were glow discharged for 20 s to render them hydrophilic. The suspension was incubated for 1 min at room temperature. Excess sample solution was removed by blotting with a filter paper touched to the edge of the grid. After removing the excess fluid, the grid was stained with 2 % (w/v) potassium phosphotungstate (KPTA) at pH = 7.0 for 60 s. Then the grid was dried at room temperature. Negatively stained specimens were examined with the Zeiss Auriga FIB-SEM microscope operated at 30 kV in STEM mode.

Cryo-Transmission Electron Microscopy (Cryo-TEM)

Cryo-TEM allows direct investigation of samples in their vitrified state at low temperature. The sample preparation for cryo-TEM technique was carried out on 200-mesh carbon-coated holey grids. Before the sample application, a glow discharge was performed in order to hydrophilize the grid for optimal spreading of the aqueous sample (Kuntsche et al. 2011). The suspension was then drop cast onto TEM grids following which the excess sample was absorbed using a filter paper, leaving a thin film of sample in the holes of the grid. Then, the grid was mounted in a Gatan cryo-plunge 3 device and immediately frozen by plunging in liquid ethane cooled by liquid nitrogen. After vitrification, the frozen-hydrated specimen was inserted to the Gatan cryo-transfer system and transferred into the TEM system. The imaging was carried out by a Zeiss Libra 200 MC TEM equipped with a model Gatan 915 cryo-specimen holder, at an acceleration voltage of 200 kV, and a temperature of about −170 °C under strict low dose conditions (<15 e Å^{-2}). Images were recorded with a Gatan UltraScan 1000XP. Quantitative analysis of $n > 30$ particles was used to measure the size of particles at each stage of solubilization.

Results and Discussion

Surfactant-Induced DPhPC Solubilization

TX-100 Interaction with DPhPC

The three stages of detergent–liposome interactions are identified as a function of increasing detergent concentrations (TX-100) from turbidity measurements on large unilamellar vesicles of DPhPC (see Fig. 2a). In stage I, detergent molecules associated with the membrane bilayer without any structural alteration of the vesicles. Initial swelling of the liposomes caused by the detergent insertion into the bilayer corresponds to the onset of solubilization. At this stage, the concentration of free detergents remains below the CMC of the pure detergent up to R_{sat} (Lichtenberg 1983) as indicated in Fig. 2a. Further increase of detergent concentration results in bilayer saturation and consequently mixed micelle formations (stage II in Fig. 2a). Beyond this stage, detergent addition results in more mixed micelle formation, which is indicated by the corresponding decrease in absorbance in the turbidity measurements. This decrease in the optical density data reaches a minimum at R_{sol}, which marks the onset of solubilization (stage III in Fig. 2a).

The different phase transitions of DPhPC liposomes observed from the abovementioned optical density measurements show excellent agreement with DLS data (see Fig. 2b, left panel). The three stages of the effect of TX-100 concentration (C_{Trit}) on DPhPC liposomes are represented by the three consecutive plots marked I, II, and III, respectively. These plots indicate that starting with intact liposomes with no TX-100, the particle size distribution (PSD in terms of number distribution, %) has a peak hydrodynamic diameter of ~90 nm. With the addition of TX-100 in the concentration ranges C_{Trit} ~ 0–2.9 mM, the peak size broadens and shifts to ~160 nm as seen from the absorbance data in Fig. 2a, indicating a swelling of the mixed detergent vesicles at the detergent concentration corresponding to R_{sat}. Beyond this point, increased detergent concentration results in a shift in the peak size (stage II in Fig. 2b, left panel) from ~160 nm (C_{Trit} = 2.3 mM) to ~15 nm (C_{Trit} = 6.0 mM) that corresponds to the stage II in Fig. 2a. Here we note that the coexistence of the second peaks at ~100–150 nm indicate the presence of mixed micelles with vesicles. The aforementioned shift into a smaller hydrodynamic diameter is due to the appearance of more mixed micelles as the concentration of

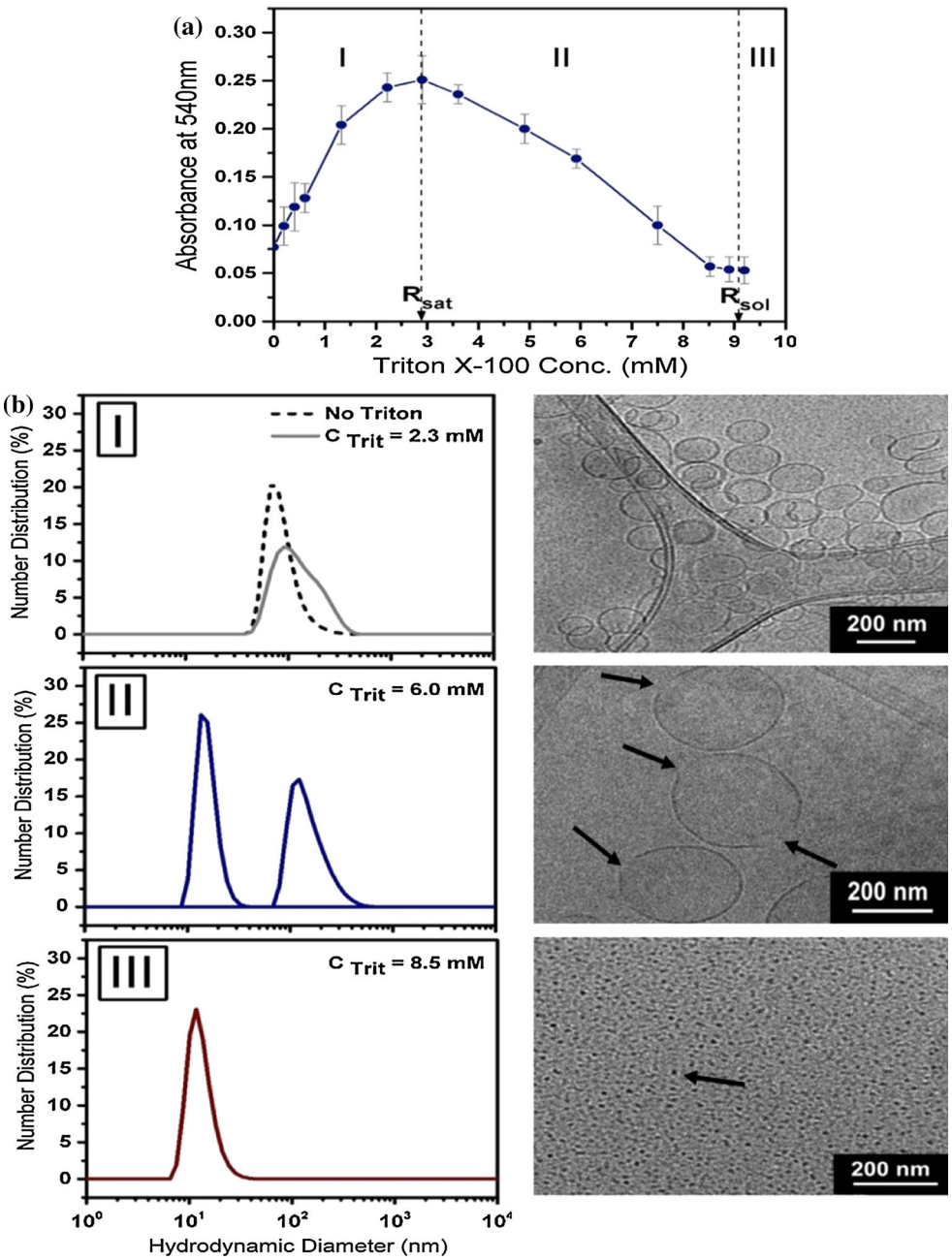

Fig. 2 Solubilization stages of preformed DPhPC liposomes at 4 mg ml^{-1} concentration induced by stepwise increase of TX-100 concentration (mM), as observed with: **a** turbidity measurements optimized for liposome adsorption at 540 nm; (**b**, *left panel*) number distribution from dynamic light scattering (DLS) and (**b**, *right panel*) corresponding cryo-TEM micrographs of each stage, indicating: *I* intact liposomes in absence of detergent; *II* liposome treated with detergent concentration above R_{sat} ($C_{Trit} = 6.2$ mM), where *arrows* indicate the open bilayer fragments, and *III* lipid-TX-100 micelles above R_{sol} ($C_{Trit} = 8.4$ mM). *Arrow* indicates the spherical mixed micelles

detergent starts approaching R_{sol} ($C_{Trit} \sim 9.2$ mM). Finally, the peak size of ~13 nm at very high detergent concentration of $C_{Trit} = 8.5$ mM in Fig. 2b, left panel (stage III) is consistent with turbidity measurements indicating the minimum optical density in stage III of Fig. 2a due to the emergence of mixed micelles.

Morphological variations corresponding to the aforementioned solubilization stages are elucidated with cryo-TEM images of liposome structures in their vitrified states that correlate very well with the different stages indicated by our turbidity and DLS measurements. Starting with intact DPhPC liposomes after extrusion through 100 nm filters, regularly shaped unilamellar liposomes with delineated 4–5 nm lipid bilayer walls are observed (stage I in Fig. 3b, right panel). Cryo-TEM images for stage I of DPhPC liposome solubilization with detergent concentrations below R_{sat} indicate the retention of the vesicular structures along with enlargement in the liposome diameter due to detergent incorporation within the membrane bilayers (refer to Figure S1, Supplementary Material). Stage II of Fig. 2b (right panel) indicates the appearance of lipid-detergent mixed micelles (~20 nm in sizes), along with stable open vesicular structures (Lichtenberg et al. 2013a; Stuart and Boekema 2007) (~150–200 nm) at

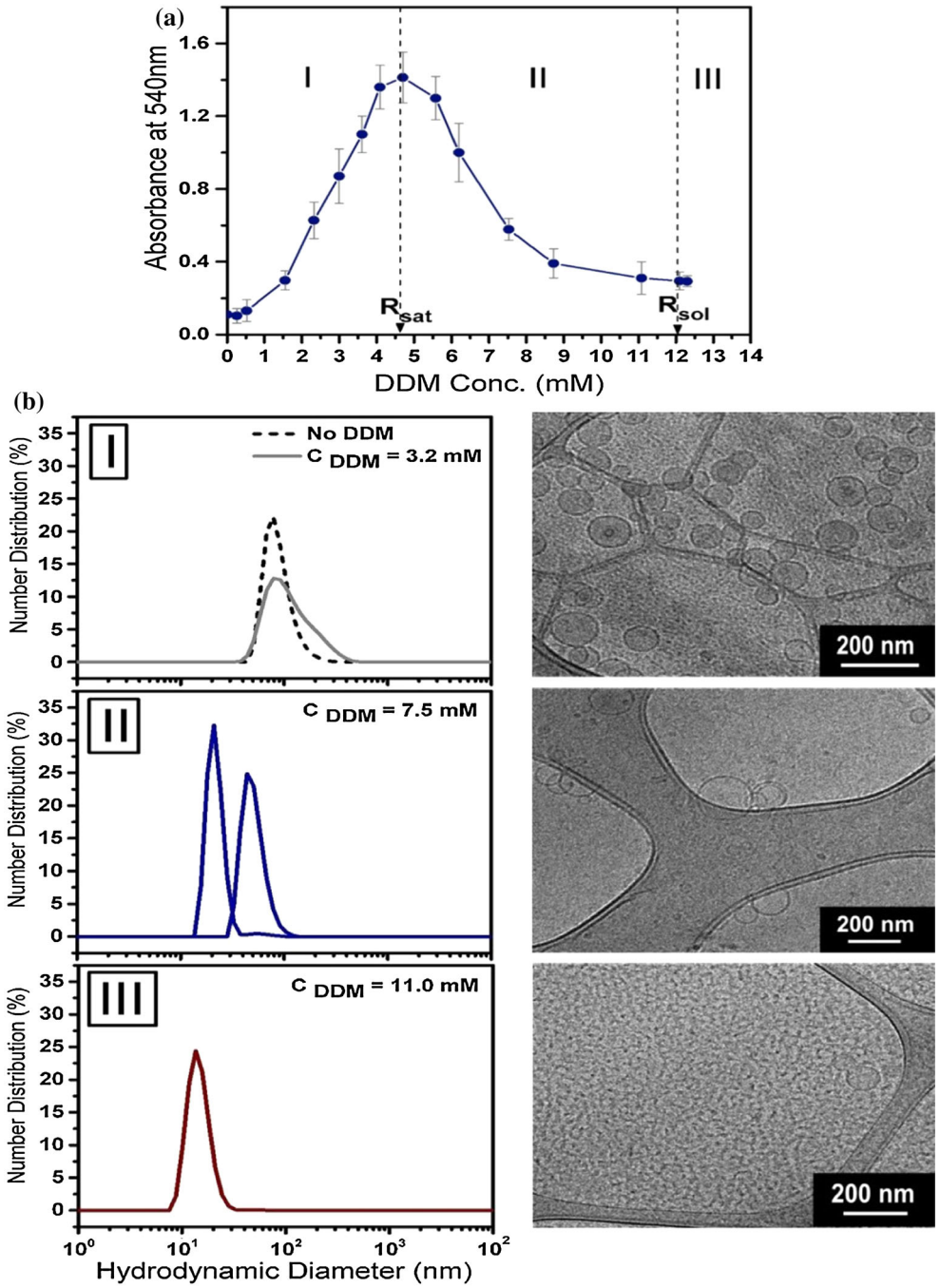

Fig. 3 Solubilization stages of preformed DPhPC liposomes at 4 mg ml^{-1} concentrations induced by stepwise increase of DDM concentration (mM) as observed with: **a** turbidity measurement; (**b**, *left panel*) number distribution from dynamic light scattering (DLS) and (**b**, *right panel*) corresponding cryo-TEM micrographs of each stage, indicating *I* intact liposomes treated with detergent concentration below R_{sat} ($C_{DDM} = 4.3$ mM); *II* mixed micelle–mixed vesicle structures above R_{sat} ($C_{DDM} = 7.0$ mM) and, *III* full solubilization of liposomes by detergent molecules and mixed micelle formation around R_{sol} ($C_{DDM} = 9.5$ mM)

$C_{Trit} \sim 6.2$ mM. This bilayer opening is associated with the rapid solubilization of bilayers by detergents with relatively small polar moiety as in the case of TX-100. Such rapid solubilization is achieved due to detergent molecules acting from both sides of the phospholipid bilayer (transbilayer solubilization) that ultimately makes them permeable and disintegrate into mixed micelles (Lichtenberg et al. 2013a; b; Stuart and Boekema 2007; Sudbrack et al. 2011). Our observations in the present study indicates that addition of TX-100 to multilamellar DPhPC vesicles

mimic the *trans*-membrane solubilization mechanism (refer to Figure S1, Supplementary Material). The above-mentioned mixed micelle formation due to detergent association is also supported by stained TEM images (refer to Figure S2, Supplementary Material). Finally, at $C_{\text{Trit}} \sim 8.4$ mM, stage III of Fig. 2b (right panel) represents the transition of the whole bilayer to spherical mixed micelles that also corresponds to stage III in Fig. 2b (left panel).

DDM Interaction with DPhPC

The turbidity measurements for DPhPC with DDM indicate the familiar three-stage solubilization curve as also observed for the TX-100 case except that the maximum absorbance value at R_{sat} is much higher for the DDM case. Specifically, the peak absorbance value at R_{sat} for the DDM case in Fig. 3a indicates a ~14-fold increase from the initial values for intact liposomes as compared to the corresponding ~3-fold increase for the TX-100 case. A stable turbidity level is reached almost instantaneously upon addition of TX-100 above R_{sat}, where for the DDM case, more than 2 h is needed to reach a stable turbidity level. Such differences in the turbidity behavior between DDM and TX-100 can be attributed to the two distinct vesicle-to-micelle transition mechanisms for these two detergents, as also reported in an earlier work of Stuart et al (Koeppe and Andersen 1996).

The saturation and solubilization points for the DPhPC-DDM systems are identified as R_{sat} at $C_{\text{DDM}} \sim 4.7$ mM and R_{sol} at $C_{\text{DDM}} \sim 12.0$ mM, respectively, along with the solubilization stages I, II, and III as marked in Fig. 3a. DLS data also confirm these stages, where stage I for the PSD in Fig. 3b (left panel) represents the shift from peak size of ~90 nm for pure lipid suspension to the peak size of ~160 nm at $C_{\text{DDM}} \sim 3.2$ mM. Absorbance measurements in Fig. 3a shows a systematic increase for DDM concentrations up to $C_{\text{DDM}} = 4.7$ mM. Beyond this point, increases in DDM concentrations are accompanied by a marked decrease in the relative absorbance (Fig. 3a), which is in agreement with DLS measurements indicating a reduction in peak sizes scattered over ~20–85 nm at $C_{\text{DDM}} \sim 7.5$ mM. This corresponds to the region of coexisting mixed micelle–mixed vesicle systems (stage II in Fig. 3b, left panel). Finally, at $C_{\text{DDM}} = 11.0$ mM, which is close to the solubilization concentration (R_{sol}) in Fig. 3a, the absorbance levels off to the minimum value, while the PSD indicates a peak size ~12 nm corresponding to only mixed micelle formation (stage III in Fig. 3b, left panel). In comparison to the TX-100-mediated solubilization of DPhPC, the solubilization process with DDM indicates a broader stage II that persists up until $C_{\text{DDM}} > 10$ mM, as seen from Fig. 3a.

Cryo-TEM images in Fig. 3b (right panel), corresponding to the DLS data in Fig. 3b (left panel) for each of the 3 stages, confirm the vesicle–micelle transitions for DPhPC treated with DDM. Intact vesicular structures of liposomes at $C_{\text{DDM}} \sim 4.3$ mM (vesicle diameter ~80–170 nm) are observed in stage I (right panel). Swelled yet, closed vesicles coexist with mixed micelle structures at $C_{\text{DDM}} \sim 7.0$ mM (size distributions ~150–180 and 20 nm) in stage II (right panel), where liposome disintegration into small worm-like mixed micelles at $C_{\text{DDM}} \sim 9.5$ mM (micelle diameter ~12 nm) are seen in stage III (right panel). These images correlate extremely well with earlier absorbance data (Fig. 3a) and PSD peaks (Fig. 3b, left panel). A few closed liposome structures were observed even at stage III of solubilization (see Fig. 3b, right panel). Closed vesicle-to-micelle transition has been attributed to the larger and polar head groups of DDM initiating a slow detergent solubilization of the bilayers. Such solubilization involves the micelles getting pinched off from outer monolayer of the vesicles. Thus, in the second stage of solubilization, (stage II) small worm-like mixed micelles coexist with closed vesicle. This mechanism is known as micellar solubilization (Lichtenberg et al. 2013a; Stuart and Boekema 2007). Previous studies on egg PC treated with DDM have revealed the formation of long string-like structures during stage II and appearance of transitional "gel-like" state at the end of stage II (Lambert et al. 1998; Knol et al. 1998). But, in our present studies with DPhPC, we only observe worm-like micelles at stage II and stage III that are below 20 nm in size. The aforementioned observations are further validated through STEM images of the solubilization stages II and III (refer to Figure S3 in Supplementary Material).

Surfactant-Induced DPPG Solubilization

TX-100 Interaction with DPPG

In the case of solubilization of DPPG liposomes with TX-100, the optical density curve in Fig. 4a peaks over a narrow range of TX-100 concentrations that correspond to R_{sat}. Moreover, unlike all the previous cases reported here, the peak absorbance is scattered over a range of TX-100 concentrations rather than a single peak value that finally equilibrates to a minimum at $C_{\text{Trit}} > 2.0$–3.0 mM. In concert with turbidity measurements, the DLS data for number and volume distributions (%), as shown in Fig. 4b (left and right panels respectively), provide information about possible arrangements of DPPG bilayer in association with TX-100. The PSD, in terms of number distribution (%), indicates a single uniform peak corresponding to a hydrodynamic diameter of ~98 nm at $C_{\text{Trit}} = 0.3$ mM (stage I in Fig. 4b, left panel). As the detergent

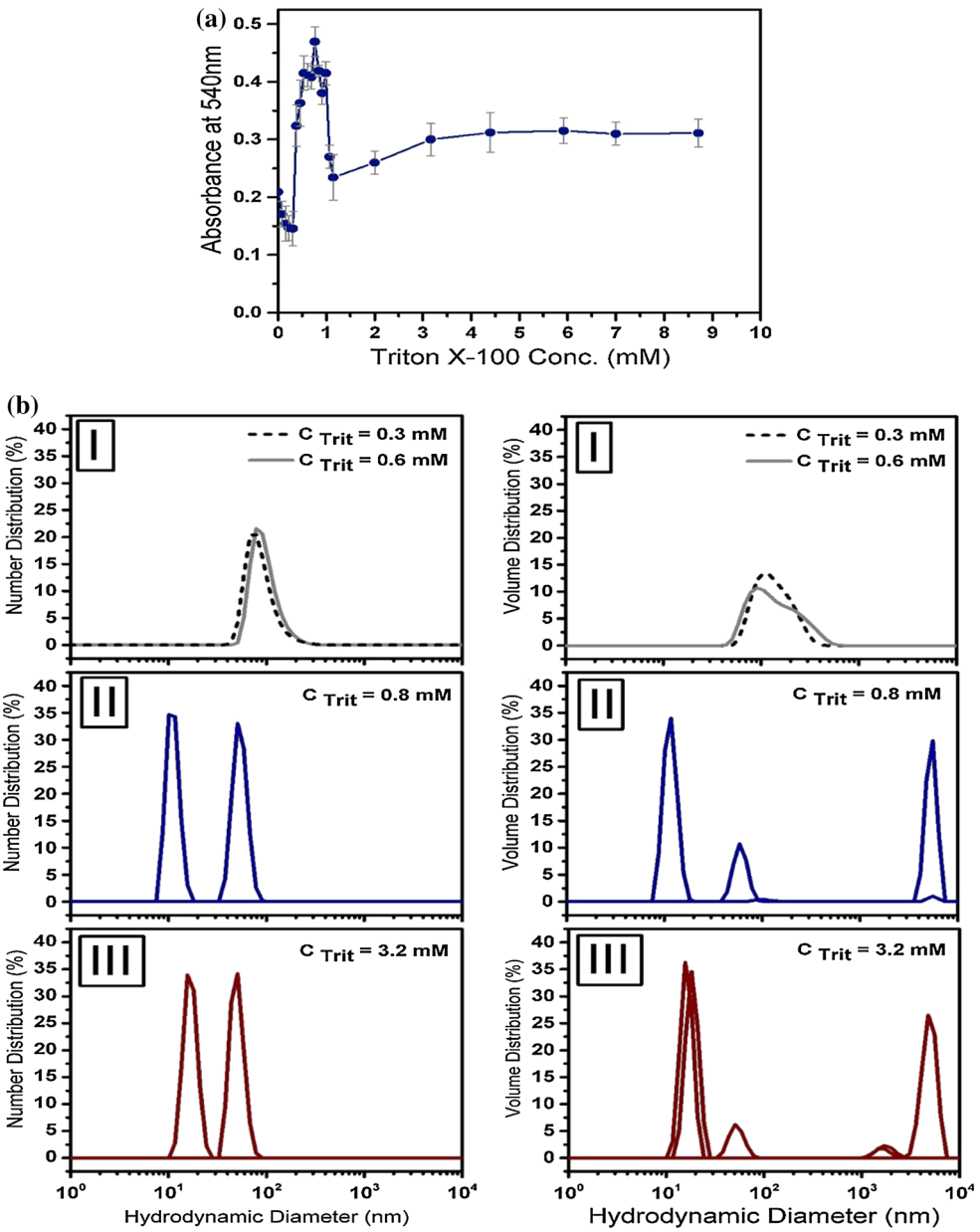

Fig. 4 Solubilization stages of preformed DPPG liposomes at 4 mg ml^{-1} concentrations induced by stepwise increase of TX-100 concentration (mM) as observed with: **a** turbidity measurement optimized; **b** number distribution (*left panel*) and volume distribution (*right panel*) (%) from dynamic light scattering (DLS) measurements for the stages *I*, *II*, and *III*

concentration is increased to $C_{\mathrm{Trit}} = 0.6$ mM, the peak size for the PSD decreases to ~88 nm. This can be interpreted as the onset of the formation of mixed micelles–vesicle system which would affect the number-averaged particle size. A further increase in TX-100 concentration to $C_{\mathrm{Trit}} = 0.8$ mM leads to the appearance of two peak sizes at ~12 and 54 nm (stage II in Fig. 4b, left panel). Finally, even at very high detergent concentrations ($C_{\mathrm{Trit}} = 3.2$ mM), the PSD in Fig. 4b (left panel) indicates two size peaks at ~16 and 50 nm (stage III). These observations contradict the existence of only mixed lipid–detergent micelles commonly observed at high detergent concentration regimes for the DPhPC systems studied earlier. To investigate these observations in detail, PSDs in volume distributions (%), in stage I of Fig. 4b (right panel), reveal the appearance of broader peak sizes spread over ~100–260 nm at $C_{\mathrm{Trit}} = 0.6$ mM. Furthermore, at $C_{\mathrm{Trit}} = 0.8$ mM (stage II in Fig. 4b, right panel), a large secondary peak appears at ~3850 nm in addition to the peaks at ~12 and 54 nm seen in Fig. 4b (stage II, left panel). These large micron-sized peaks persist even at $C_{\mathrm{Trit}} = 3.2$ mM concentration where the absorbance in Fig. 4a plateaus out. It should be highlighted that these large peak sizes are only observed in volume weighted size distributions and not in the number weighted size distributions, thereby indicating the presence of a relatively small population of larger structures in the abovementioned cases since the number-average particle size is mainly

influenced by the larger population of smaller particles. Here, our hypothesis is that the vesicular DPPG liposomes, when solubilized with TX-100, are thermodynamically favored to undergo structural disruption and phase transition into extremely large and more complex network of structures. The increasing formation of these structures is also possibly indicated by the increase in the absorbance value beyond $\sim$3.5 mM that subsequently levels off beyond 4 mM concentration possibly due to the attainment of equilibrium structures.

The aforementioned hypothesis is verified with the aid of cryo-TEM images to understand this anomalous behavior of the process that might be leading to the proposed larger structures with complex morphology. Our results indicate that the regular spherical shaped vesicular liposome structures, with an approximate diameter of $\sim$100 nm in the absence of TX-100 (Fig. 5a), undergo structural rearrangements upon addition of TX-100 to form a network of complex structures. Here, twisted, dendritic structures with 200–500 nm length are observed (seen from Fig. 5b) at ($C_{\mathrm{Trit}} = 0.61$ mM). This structural change also agrees well with the peak broadening in the PSD in stage I of Fig. 4b (right panel). Upon further increase of detergent concentration ($C_{\mathrm{Trit}} \sim$ 0.75–0.8 mM), these twisted dendritic structures unravel to form micron-sized cylinders, as seen from Fig. 5c, that corresponds to the dominant micron-sized peak in stage II of Fig. 4b (right panel). These open cylindrical structures persist even at higher concentration, thereby explaining the existence of the micron-sized peaks in stage III of Fig. 4b (right panel). To validate the proposed explanation for the abovementioned phenomenon, the vesicle solubilization process is further analyzed using the STEM technique that indeed shows the loss of vesicle structures to twisted tubular structures with inner helical pitch of $\sim$100 nm along with twist interval of $\sim$1150 nm and a diameter of $\sim$180 nm at $C_{\mathrm{Trit}} = 0.61$ - mM (Fig. 5b, inset). Finally, a further addition of TX-100 ($C_{\mathrm{Trit}} = 0.8$ mM) induces bifurcation of these lipid tubules into long dendritic, helical structures (pitch $\sim$480 nm and diameter $\sim$120 nm) with a filament radius of $\sim$40 nm (Fig. 5c, inset), which corroborates our cryo-TEM images.

It is noted that the DPPG/TX-100 interactions at room temperature led to the aforementioned complex structures (as observed via TEM micrograms). In order to investigate the role of kinetics and/or thermodynamics in the formation of these structures, the structural arrangements in the solution were studied at 50 °C, above the transition temperature of DPPG at 41 °C. DLS data and cryo-TEM images show shift of micron-sized structure found at 25 °C to smaller structures (17–210 nm) at 50 °C (refer to Figure S4 in Supplementary Material). Our hypothesis here is that although we started with DPPG lipid in the fluid state, addition of TX-100 causes the system to undergo a phase change and become kinetically trapped at room

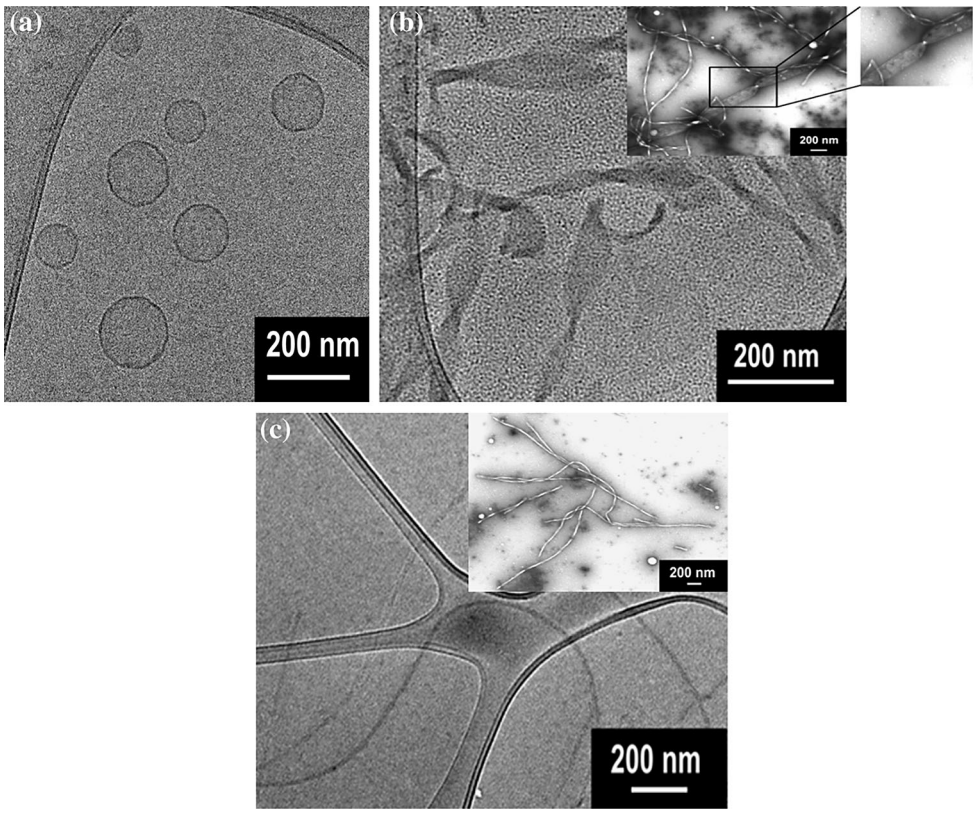

Fig. 5 Cryo-TEM micrographs along with stained TEM images (*insets*) representing solubilization of preformed DPPG liposomes with TX-100 indicating: **a** intact liposomes in the absence of detergents; **b** transition from vesicular structures to twisted, tubular (ribbon-like) structures at $C_{\mathrm{Trit}} = 0.61$ mM, and **c** bifurcation of lipid tubes into long dendritic, helical (or, spiral) structure at $C_{\mathrm{Trit}} = 0.8$ mM

temperature (25 °C), where the complex micron-sized structures formed are not equilibrium structures. Reaction kinetics is partially a function of the stability of the intermediate species (and transition states). To this end, the pathway of a chemical reaction *en route* to its final products has to overcome the transition states. If these intermediates are highly unstable (i.e., highly energetic) relative to the initial reactants, then the initial barrier of activation energy that must be surpassed to set the reaction in motion will be relatively high, and the reaction will tend to proceed slowly (if at all). In such a scenario, the onward reaction rates for the formation of the final products would be highly retarded, thereby kinetically trapping the intermediate (transition) state. These complex tubular structures represent the transition states and were observed to persist even after 2 weeks (data not shown here). To this end, increasing the temperature to 50 °C provides the activation energy required for the vesicle–micelle transition.

It needs to be highlighted here that previous studies on the solubilization of gel phase membranes have identified two distinct situations for solubilizations above and below the transition temperature. Above transition temperature, the various lipids behave similarly, and the respective solubilization data follow the three-stage transition model. However, below transition temperature, two scenarios can be detected: (1) when temperature is relatively close to the transition temperature of the pure lipid, bilayers were found to be solubilized by TX-100 (Ribeiro and Dennis 1974). In fact, these lipids are solubilized by a lower concentration of TX-100 as compared to the bilayers in fluid phase (Patra et al. 1998; Alonso et al. 1981). This is due to the coexistence of two phases: a fluid phase and a gel phase. This mixed phase (liquid-ordered phase) explains many of the unusual material properties of two-phase membranes; (2) when temperatures are well below the transition temperature, lipids in the gel state cannot be solubilized by the detergent (Ribeiro and Dennis 1974; London and Brown 2000). Our current results for DDPG/TX-100 system also corroborate these observations wherein, for the same concentration of TX-100, DPPG vesicles were found to be soluble in TX-100 in the fluid state (at ∼50 °C) but were insoluble in the gel state (at 25 °C) (refer to Figure S4 in Supplementary Material).

DDM Interaction with DPPG

In continuation with the aforementioned study, the optical density measurements for DPPG, treated with different concentrations of DDM also indicate the familiar three-stage solubilization curve with R_{sat} at $C_{DDM} = 0.6$ mM and R_{sol} at $C_{DDM} = 1.2$ mM (stages I, II and III as shown in Fig. 6a). DLS data also confirm these stages, where the PSD at $C_{DDM} = 0.3$ mM show a peak size of ∼85 nm, representing the intact DPPG vesicle size that increase to ∼100 nm upon addition of DDM ($C_{DDM} = 0.6$ mM corresponding to R_{sat} in stage I of Fig. 6a), indicating swelling of the DPPG vesicles (stage I in Fig. 6b, left panel). In the coexistence region (stage II in Fig. 6a), the PSDs exhibit a scatter over a size range of <7 nm (DDM micelle size ∼5.5–6 nm) up to >45 nm (stage II in Fig. 6b, left panel). This can be attributed to the mixed vesicle–mixed micelle inter-conversions. Finally, at detergent concentrations above R_{sol} in Fig. 6a ($C_{DDM} = 1.4$ mM), the PSD represents peaks ranging from <2 nm up to >11 nm, which corresponds to mixed micelle formation (stage III in Fig. 6b, left panel).

Cryo-TEM images of DPPG solubilization with DDM are found to be in agreement with aforementioned results, where general structure of liposomes remains intact during stage I and II of solubilization as seen from Fig. 6b (right panel). These images demonstrate a sharp contrast to the results obtained with liposomes titrated with TX-100. During the solubilization, DDM associated with the DPPG bilayer and a general structure of liposomes remains intact at stage I of solubilization (see Fig. 6b, right panel). Bifurcation of lipid and helical or spiral structure arrangement has not been seen at DDM concentrations that are far beyond R_{sat} (see stage II, right panel), and, even at relatively high detergent/lipid ratios, the lipids still tended to form liposomal structures despite the relatively high concentration of DDM in the bilayers (see stage III, right panel). Mixed micelles are formed upon further increase of detergent concentration beyond R_{sol}, where neither liposomes nor any dendritic structures are observed any longer. The faceted morphologies that we see in the TEM images were reproducible and attributed to the incorporation of detergents into the liposomes in a way that alters their local bending rigidity and curvature. It has been shown that membrane domains enriched in saturated sphingolipids and cholesterol (lipid rafts) show membrane deformation due to the fact that cholesterol induces profound changes in the mechanical properties and conformational states of some types of lipid bilayers (Levitan et al. 2000; Sanat et al. 2005). This observation is also consistent with studies on solubilization of giant unilamellar vesicles (GUVs) which have shown that some detergents mechanically destabilize the membrane through curvature stress, resulting in curvature-induced instability (Sudbrack et al. 2011; Babnik et al. 2003).

Discussion on the Choice of Detergents and Liposomes for Proteoliposome Preparation

The aforementioned characterizations need to be contextualized in the framework of our motivations for the present study, namely the efficacy of membrane protein

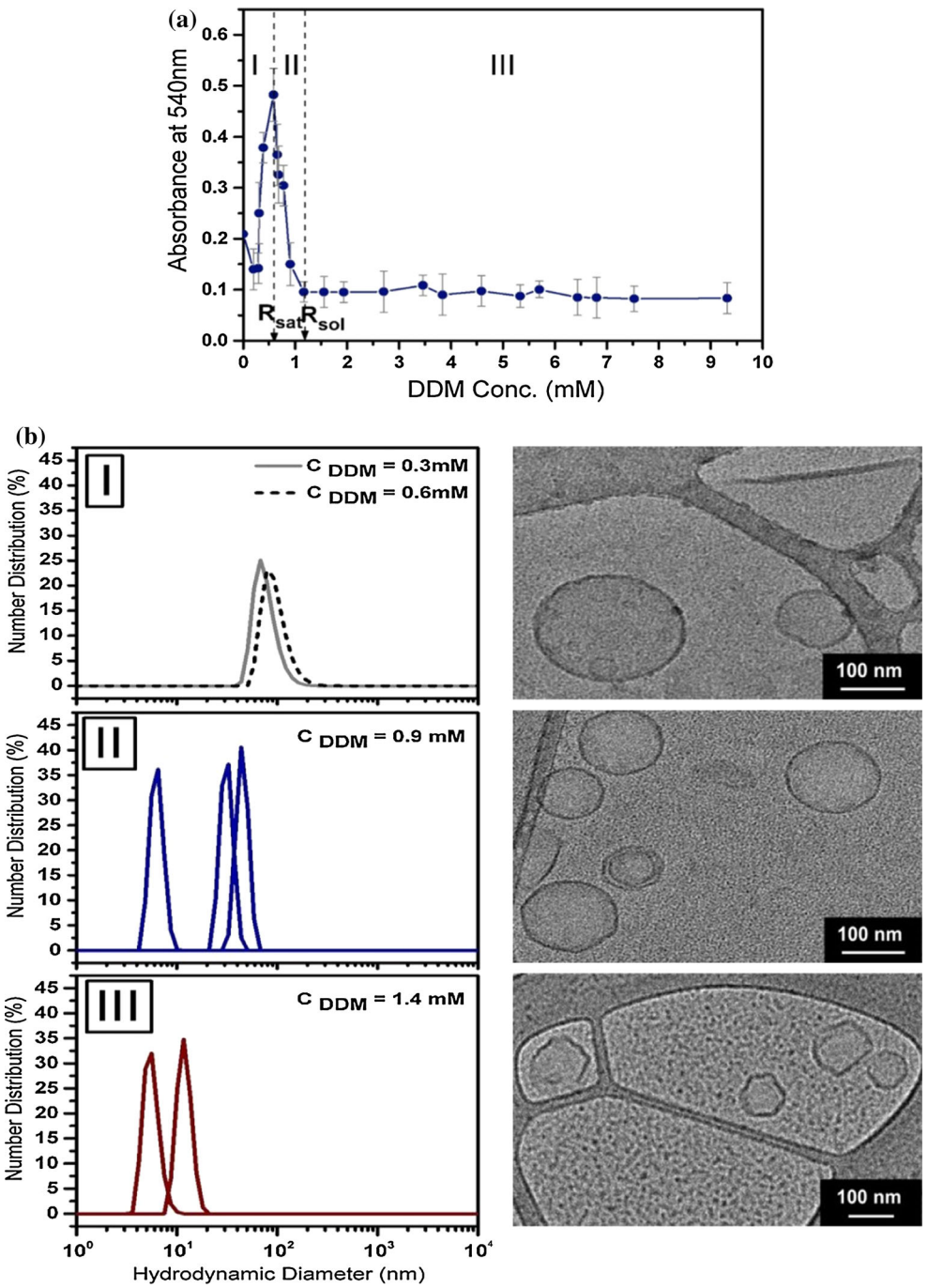

Fig. 6 Solubilization stages of preformed DPPG liposomes at 4 mg ml^{-1} concentrations induced by stepwise increase of DDM concentration (mM) as observed with: **a** turbidity measurement; (**b**, *left panel*) number distribution (%) from dynamic light scattering (DLS) measurements, and (**b**, *right panel*) corresponding cryo-TEM micrographs of each stage, indicating *I* liposome treated with detergent concentration below R_{sat} ($C_{DDM} = 0.4$ mM), where liposome structure remains intact; *II* coexistence stage of solubilization ($C_{DDM} = 0.8$ mM); *III* high population of mixed micelles and smaller liposomes close to R_{sol} ($C_{DDM} = 1.2$ mM)

reconstitution into suitable bio-mimetic lipid membrane systems. The choices of the lipids studied here are based on (1) the predominant presence of PG in thylakoid membrane of PS I, and (2) the thermal and structural stability of DPhPC that makes it suitable as highly stable and leak free membranes in membrane-based assemblies (Baba et al. 1999). In an effort to explain the rationale behind our choices of the specific lipid membranes, namely DPhPC and DPPG, we dedicate this section toward discussing some of the structural and phase characteristics of the

aforementioned lipids that, in turn, provides fundamental insights into the interpretation of our results presented here.

The differences in the specific behaviors of how TX-100 partitions into DPhPC and DPPG bilayers can be explained on the basis of the structural differences, as well as the role of electrostatic charge and the thermotropic state of the lipid relative to the transition temperature. To this end, the mismatch between the lateral areas of the headgroups and the hydrocarbon chains of the two lipids under study can provide a plausible explanation to the differences in their solubilization behaviors. While DPhPC has a larger headgroup (volume 319 $Å^3$) than DPPG (volume 257 $Å^3$), the tail groups of both lipids have 16-carbon long hydrocarbon chains that are methyl-branched in the case of DPhPC but has no methyl branches in the case of DPPG. Such branched-chain structures affect the structures of the lipid membranes formed such that DPhPC monolayers exhibit a lateral area per lipid of $\sim$80 $Å^2$ at 25 °C while lipids with similar chain lengths, but devoid of methyl groups, exhibit lower molecular areas (e.g., dipalmitoylphosphatidylcholine with 47.4 $Å^2$ and dipalmitoylphosphatidylcholine with 65.8 $Å^2$) even at the tightest packing conditions (Yasmann and Sukharev 2015). In contrast, the area/lipid for DPPG in the gel phase (46.7 $Å^2$ at 25 °C) is smaller than that reported for DPhPC (Pabst et al. 2007). DPPG molecules are able to tightly pack with the tails arranged in a hexagonal fashion at high surface pressure, unlike the DPhPC molecules that are not able to do so due to the head–tail mismatch, causing their tailgroups to be tilted even at high surface pressures (London and Brown 2000; Ege and Lee 2004). Such tightly packed structures for DPPG molecules can possibly explain the inability of TX-100 molecules to effectively solubilize the DPPG lipid bilayers, thereby resulting in the complex ribbon-like structures (as seen earlier in Fig. 5b, c).

Moreover, the electrostatic charge might play a significant role in the differences observed. Recent work of Ahyayauch et al. (2012) on solubilization of dipalmitoylphosphatidylcholine (DPPC) membranes with TX-100 above and below lipid transition temperature shows that TX-100 can solubilize the DPPC bilayers in the gel phase (at 20 °C) as well as in fluid phase (at 50 °C). Furthermore, these lipid bilayers at gel phase were solubilized by a lower concentration of TX-100 as compared to the bilayers in fluid phase. DPPC, analogous to DPPG, has a 16-carbon long hydrocarbon chain that has no methyl branches. DPPC is also tilted and arranged in a hexagonal lattice in the gel phase, and also has its gel-to-liquid crystalline transition temperature at $\sim$41 °C. However, our results for DPPG/TX-100 system appear to contradict this scenario, where DPPG vesicles were soluble in TX-100 in the fluid phase but were insoluble in the gel phase. Considering that DPPC has the same head group as DPhPC, the only differences between the two remain in DPPC being a non-ionic lipid while DPPG is an anionic lipid. Hence, the aforementioned differences in solubilization behavior can possibly be attributed to the different electrostatic charge interactions of the two lipids.

Finally, the temperature effects, while influencing the thermal motion of the molecules, are also responsible for the gel-fluid thermotropic transitions in the case of DPPG. Thus, the stable fluid state of DPhPC over wide temperature ranges and the gel-to-fluid phase transitions for DPPG at $\sim$41 °C might be critical in explaining the variations in the interactions of TX-100 with DPPG above and below the transition temperatures. It needs to be mentioned here that despite the larger and more polar headgroups of DDM molecules as compared to those for TX-100, DDM appears to effectively solubilize the DPPG lipid bilayers. In contrast, TX-100 seems to promote a tighter packing of the lipids that appears to result in a kinetically trapped system not in thermal equilibrium. Our current hypothesis is that the addition of TX-100 to the DPPG vesicle suspensions may alter the balance between headgroup and hydrocarbon chain interactions to create a transition state of DPPG. In such transition states, the lipids can undergo a denser packing owing to possible tilting of the DPPG headgroups out of the bilayer plane in response to the increasing fluctuation pressure from the hydrocarbon chains (Patra et al. 1998; Ege and Lee 2004). In future, a detailed validation of this hypothesis would require a molecular level investigation into the structural arrangements of these systems.

In regard to most membrane protein reconstitutions, the success rates are proven to be low at detergent concentrations below the saturation point R_{sat} where the liposomes are not fully saturated with the detergent molecules (Rigaud et al. 1995; Knol et al. 1998) or above the solubilization point R_{sol}, where protein reconstitution most often results in a greater amount of protein association with detergent micelles and less reproducible orientation in lipid vesicles (Knol et al. 1998). Past literatures have reported that protein incorporation in the membrane is highest at stage II (refer to Fig. 1), where detergents disrupt lipid–lipid interactions and enhance the bilayer permeability (Geertsma et al. 2008; Lambert et al. 1998; Knol et al. 1998; Seddon et al. 2004).

The significant findings from our solubilization studies of DPhPC and DPPG with DDM and TX-100 are summarized in Table 1. It highlights the critical morphological characteristics of the liposome structures that indicate the suitable phase windows for protein insertion. Considering that most successful protein incorporations occur in stage II, the aforementioned observations suggest that DDM-destabilized DPhPC liposomes provide the widest detergent concentration range over stage II for protein insertion.

Table 1 Highlights of the overall significant findings

		R_{sat} (mM)	R_{sol} (mM)	Observed structure	Possible window of protein insertion
DPhPC	TX-100	2.9	Above 8.0	Regular III stage transition	wide window at stage II
DPhPC	DDM	4.7	Above 11.0	Regular III stage transition	Wider window at stage II
DPPG	TX-100	–	–	Irregular structures, kinetically trapped (tubular, helical and spiral)	Inapplicable
DPPG	DDM	0.6	1.2	Regular III stage transition	Narrow window at stage II

The DPhPC/TX-100 system follows it closely as a possible candidate for protein insertions.

The stage II of solubilization with TX-100 is limited between $C_{Trit} \sim 2.9$—above 8.0 mM, where the same with DDM extends over $C_{DDM} \sim 4.7$ mM—above 11.0 mM. Such effects are also observed for solubilizations with different lipid concentrations (refer to Figure S5, Supplementary Material). While the wider insertion window for DDM might be helpful in the easier implementation of proteoliposome preparation, the slightly lower detergent requirements for TX-100 might make the process more efficient and economically viable. Furthermore, the highly irregular structural arrangements arising out of kinetically trapped TX-100/DPPG system at room temperature indicate their uncertainty for successful protein insertion. It needs to be pointed out here that the charges carried by the lipid head groups (DPPG is negatively charged and DPhPC is zwitterionic) cannot substantiate the unique lipid-detergent solubilization behavior for DPPG/TX-100 system. To this end, in spite of both TX-100 and DDM being non-ionic detergents, the solubilization of DPPG with DDM does not show the complex structures as observed for the TX-100 case. Studies are currently underway to further investigate the implications of these complex structures in terms of PS I encapsulation process. Finally, our results show that DDM-destabilized DPPG liposomes exhibit a narrower window of detergent concentrations ($C_{DDM} \sim 0.6$–1.2 mM) for protein insertion in stage II of the solubilization process.

Conclusions

In this article, an in-depth investigation of surfactant-induced membrane solubilization of two phospholipids (DPhPC and DPPG) by two detergents (DDM and TX100) commonly used for protein solubilization is presented. Our results from the current study indicate that DPhPC liposomes maintain their vesicular structures intact at the initial stages of detergent addition. Furthermore, when solubilized with both TX-100 and DDM, the vesicles undergo the typical three-stage transition to the final micellar stages via mixed vesicles–micelles state. Vesicular structure formation is a result of hydration and steric forces upon amphiphiles' head groups. These forces result in a high rotational degree of freedom for the monomers and low aspect ratios during the head group interactions (Sorrenti et al. 2013), as also observed in the case of the solubilization of DPhPC liposomes. On the other hand, the stereochemistry and molecular structure of amphiphiles might result in the formation of organized supramolecular nanostructures with high aspect ratios. It has been demonstrated that some amphiphiles self-assemble into high aspect ratio structures due to the presence of one or more chiral carbons and moieties suitable for intermolecular directional interactions, such as hydrogen bonds (often secondary amide groups) (Sorrenti et al. 2013). Thus, our investigations indicate that although DPPG liposomes self-assemble in vesicular arrangements upon extrusion, the introduction of detergent, specifically TX-100, can cause structural deformation that re-organizes the vesicles into complex network of micro- and nanostructural arrangements of lipid bilayers. These structures are found to be kinetically trapped that can be energetically driven to form mixed micelles upon heating the system above the transition temperature of DPPG ($\sim$41 °C). Previous crystallographic structural studies of PS I at 2.5 Å resolution have identified four lipids consisting of three phosphatidylglycerol (PG) molecules and one monogalactosyldiacylglycerol (MDGD) molecule that are largely responsible for the long-term stability and functionality of PS I (Golbeck 2006). In light of the larger PG content in PS I lipid structures, our results for the surfactant-induced membrane solubilization of DPPG lipids provide valuable insight for our future work on developing rational and robust approaches for large membrane protein reconstitution that can lead to successful PS I-proteoliposome formation.

Supplementary Material

These materials are available free of charge via the Internet:

(a) Cryo-TEM images of different stages of DPhPC/TX-100 solubilization proving the *trans*-membrane solubilization;

(b) STEM images of DPhPC liposomes titrated with TX-100 at stage II of the solubilization;
(c) STEM images of DPhPC liposomes titrated with DDM at stage II & III of the solubilization;
(d) Volume distribution from dynamic light scattering (DLS) and corresponding cryo-TEM micrographs revealing the effect of temperature on the morphological arrangement of DPPG/TX-100 mixture;
(e) Turbidity measurements revealing the dependence of R_{sat} and R_{sol} on the choice of detergent and lipid concentration; and
(f) Physical properties of the detergents, TX-100, and DDM.

Acknowledgments The authors would like to acknowledge the University of Tennessee Advanced Microscopy and Imaging Center for instrument use, scientific and technical assistance. This work was funded by Sustainable Energy Education and Research Center (SEERC) at University of Tennessee, Knoxville.

References

Ahyayauch H, Collado MI, Alonso A, Goñi FM (2012) Lipid bilayers in the gel phase become saturated by Triton X-100 at lower surfactant concentrations than those in the fluid phase. Biophys J 102:2510–2516

Alonso A, Villena A, Goñi FM (1981) Lysis and reassembly of sonicated lecithin vesicles in the presence of triton X-100. FEBS Lett 123:200–204

Andersson M, Jackman J, Wilson D, Jarvoll P, Alfredsson V, Okeyo G, Duran R (2011) Vesicle and bilayer formation of diphytanoylphosphatidylcholine (DPhPC) and diphytanoylphosphatidylethanolamine (DPhPE) mixtures and their bilayers' electrical stability. Colloids Surf B 82:550–561

Arnulphi C, Sot J, García-Pacios M, Arrondo J-LR, Alonso A, Goñi FM (2007) Triton X-100 partitioning into sphingomyelin bilayers at subsolubilizing detergent concentrations: effect of lipid phase and a comparison with dipalmitoylphosphatidylcholine. Biophys J 93:3504–3514

Baba T, Toshima Y, Minamikawa H, Hato M, Suzuki K, Kamo N (1999) Formation and characterization of planar lipid bilayer membranes from synthetic phytanyl-chained glycolipids. Biochim Biophy Acta BBA Biomembr 1421:91–102

Babnik B, Miklavčič D, Kandušer M, Hägerstrand H, Kralj-Iglič V, Iglič A (2003) Shape transformation and burst of giant POPC unilamellar liposomes modulated by non-ionic detergent C12E8. Chem Phys Lipids 125:123–138

Bayley H, Cronin B, Heron A, Holden MA, Hwang WL, Syeda R, Thompson J, Wallace M (2008) Droplet interface bilayers. Mol BioSyst 4:1191–1208

Cladera J, Rigaud JL, Bottin H, Dunach M (1996) Functional reconstitution of photosystem I reaction center from cyanobacterium Synechocystis sp PCC6803 into liposomes using a new reconstitution procedure. J Bioenerg Biomembr 28:503–515

Cladera J, Rigaud JL, Villaverde J, Dunach M (1997) Liposome solubilization and membrane protein reconstitution using Chaps and Chapso. Eur J Biochem 243:798–804

Coelfen H, Harding SE, Boulter JM, Watts A (1996) Hydrodynamic examination of the dimeric cytoplasmic domain of the human erythrocyte anion transporter, band 3. Biophys J 71:1611–1615

De Carlo S, Harris JR (2011) Negative staining and cryo-negative staining of macromolecules and viruses for TEM. Micron 42:117–131

Deamer D, Bangham AD (1976) Large volume liposome by an ether vaporization method. Biochim Biophys Acta 443:629–634

Douce R, Holtz RB, Benson AA (1973) Isolation and properties of envelope of spinach chloroplasts. J Biol Chem 248:7215–7222

Ege C, Lee KYC (2004) Insertion of azlzheimer's Aβ40 peptide into lipid monolayers. Biophys J 87:1732–1740

Gaillard I, Slotboom DJ, Knol J, Lolkema JS, Konings WN (1996) Purification and reconstitution of the glutamate carrier GltT of the thermophilic bacterium *Bacillus stearothermophilus*. Biochemistry 35:6150–6156

Geertsma ER, Mahmood N, Schuurman-Wolters GK, Poolman B (2008) Membrane reconstitution of ABC transporters and assays of translocator function. Nat Protoc 3:256–266

Gennis RB (1989) Biomembranes: molecular structure and function. Springer, New York

Golbeck JH (2006) Photosystem I: the light-driven plastocyanin: ferredoxin oxidoreductase. Springer, New York

Gombos Z, Wada H, Varkonyi Z, Los DA, Murata N (1996) Characterization of the Fad12 mutant of Synechocystis that is defective in Δ12 acyl-lipid desaturase activity. Biochim Biophys Acta Lipids Lipid Metab 1299:117–123

Hagting A, Velde JVD, Poolman B, Konings WN (1997) Membrane topology of the di- and tripeptide transport protein of *Lactococcus lactis*. Biochemistry 36:6777–6785

Hayat MA, Miller SE (1990) Negative staining. McGraw-Hill, New York

Heerklotz H, Seelig J (2000) Correlation of membrane/water partition coefficients of detergents with the critical micelle concentration. Biophys J 78:2435–2440

Helenius A, Simons K (1975) Solubilization of membranes by detergents. Biochim Biophys Acta 415:29–79

Helenius A, McCaslin DR, Fries E, Tanford C (1979) Properties of detergents. Methods Enzymol 56:734–749

Hsieh CH, Sue SC, Lyu PC, Wu WG (1997) Membrane packing geometry of diphytanoylphosphatidylcholine is highly sensitive to hydration: phospholipid polymorphism induced by molecular rearrangement in the headgroup region. Biophys J 73:870–877

Knol J, Sjollema K, Poolman B (1998) Detergent-mediated reconstitution of membrane proteins. Biochemistry 37:16410–16415

Koeppe RE, Andersen OS (1996) Engineering the gramicidin channel. Annu Rev Biophys Biomol Struct 25:231–258

Konovalov O, Myagkov I, Struth B, Lohner K (2002) Lipid discrimination in phospholipid monolayers by the antimicrobial frog skin peptide PGLa. A synchrotron X-ray grazing incidence and reflectivity study. Eur Biophy J 31:428–437

Kragh-Hansen U, le Maire M, Moller JV (1998) The mechanism of detergent solubilization of liposomes and protein-containing membranes. Biophys J 75:2932–2946

Kuntsche J, Horst JC, Bunjes H (2011) Cryogenic transmission electron microscopy (cryo-TEM) for studying the morphology of colloidal drug delivery systems. Int J Pharm 417:120–137

Lambert O, Levy D, Ranck J-L, Leblanc G, Rigaud J-L (1998) A new "gel-like" phase in dodecyl maltoside–lipid mixtures: implications in solubilization and reconstitution studies. Biophys J 74:918–930

Levine YK, Bailey AI, Wilkins MHF (1968) Multilayers of phospholipid biomolecular leaflets. Nature 220:577–578

Levitan I, Christian AE, Tulenko TN, Rothblat GH (2000) Membrane cholesterol content modulates activation of volume-regulated anion current in bovine endothelial cells. J Gen Physiol 115:405–416

Lévy D, Gulik A, Bluzat A, Rigaud J-L (1992) Reconstitution of the sarcoplasmic reticulum Ca^{2+}-ATPase: mechanisms of

membrane protein insertion into liposomes during reconstitution procedures involving the use of detergents. Biochim Biophys Acta BBA Biomembr 1107:283–298

Lichtenberg D, Barenholz Y (2006) Liposomes: preparation, characterization, and preservation, methods of biochemical analysis. Wiley, New York

Lichtenberg D, Robson RJ, Dennis EA (1983) Solubilization of phospholipids by detergents structural and kinetic aspects. Biochim Biophys Acta BBA Rev Biomembr 737:285–304

Lichtenberg D, Opatowski E, Kozlov MM (2000) Phase boundaries in mixtures of membrane-forming amphiphiles and micelle-forming amphiphiles. Biochim Biophys Acta BBA Biomembr 1508:1–19

Lichtenberg D, Ahyayauch H, Goni FM (2013a) The mechanism of detergent solubilization of lipid bilayers. Biophys J 105:1090

Lichtenberg D, Ahyayauch H, Alonso A, Goñi FM (2013b) Detergent solubilization of lipid bilayers: a balance of driving forces. Trends Biochem Sci 38:85–93

Lindsey H, Petersen NO, Chan SI (1979) Physicochemical characterization of 1,2-diphytanoyl-sn-glycero-3-phosphocholine in model membrane systems. Biochim Biophys Acta BBA Biomembr 555:147–167

Lohner K, Latal A, Degovics G, Garidel P (2001) Packing characteristics of a model system mimicking cytoplasmic bacterial membranes. Chem Phys Lipids 111:177–192

London E, Brown DA (2000) Insolubility of lipids in Triton X-100: physical origin and relationship to sphingolipid/cholesterol membrane domains (rafts). Biochim Biophys Acta BBA Biomembr 1508:182–195

Lopez O, Cocera M, Wehrli E, Parra JL, de la Maza A (1999) Solubilization of liposomes by sodium dodecyl sulfate: new mechanism based on the direct formation of mixed micelles. Arch Biochem Biophys 367:153–160

Lopez O, Cocera M, Coderch L, Parra JL, Barsukov L, de la Maza A (2001) Octyl glucoside-mediated solubilization and reconstitution of liposomes: structural and kinetic aspects. J Phys Chem B 105:9879–9886

Lovejoy B, Akerfeldt KS, Degrado WF, Eisenberg D (1992) Crystallization of proton channel peptides. Protein Sci 1:1073–1077

Mendiolamorgenthaler L, Eichenberger W, Boschetti A (1985) Isolation of chloroplast envelopes from chlamydomonas—lipid and polypeptide composition. Plant Sci 41:97–104

Milhiet P-E, Gubellini F, Berquand A, Dosset P, Rigaud J-L, Le Grimellec C, Levy D (2006) High-resolution AFM of membrane proteins directly incorporated at high density in planar lipid bilayer. Biophys J 91:3268–3275

Morrow MR, Temple S, Stewart J, Keough KMW (2007) Comparison of DPPC and DPPG environments in pulmonary surfactant models. Biophys J 93:164–175

Mukherjee D, May M, Vaughn M, Bruce BD, Khomami B (2010) Controlling the morphology of photosystem I assembly on thiol-activated Au substrates. Langmuir 26:16048–16054

Mukherjee D, May M, Khomami B (2011a) Detergent-protein interactions in aqueous buffer suspensions of Photosystem I (PS I). J Colloid Interface Sci 358:477–484

Mukherjee D, Vaughn M, Khomami B, Bruce BD (2011b) Modulation of cyanobacterial photosystem I deposition properties on alkanethiolate Au substrate by various experimental conditions. Colloids Surf B Biointerfaces 88:181–190

Nazari M, Kurdi M, Heerklotz H (2012) Classifying surfactants with respect to their effect on lipid membrane order. Biophys J 102:498–506

Pabst G, Danner S, Karmakar S, Deutsch G, Raghunathan VA (2007) On the propensity of phosphatidylglycerols to form interdigitated phases. Biophys J 93:513–525

Parmar MM, Edwards K, Madden TD (1999) Incorporation of bacterial membrane proteins into liposomes: factors influencing protein reconstitution. Biochim Biophys Acta BBA Biomembr 1421:77–90

Pata V, Ahmed F, Discher DE, Dan N (2004) Membrane solubilization by detergent: resistance conferred by thickness. Langmuir 20:3888–3893

Paternostre MT, Roux M, Rigaud JL (1988) Mechanisms of membrane protein insertion into liposomes during reconstitution procedures involving the use of detergents. 1. Solubilization of large unilamellar liposomes (prepared by reverse-phase evaporation) by Triton X-100, octyl glucoside, and sodium cholate. Biochemistry 27:2668–2677

Patra SK, Alonso A, Goñi FM (1998) Detergent solubilisation of phospholipid bilayers in the gel state: the role of polar and hydrophobic forces. Biochim Biophys Acta BBA Biomembr 1373:112–118

Ribeiro AA, Dennis EA (1974) Effect of thermotropic phase transitions of dipalmitoylphosphatidylcholine on the formation of mixed micelles with Triton X-100. Biochim Biophys Acta BBA Biomembr 332:26–35

Rigaud JL, Levy D (2003) Reconstitution of membrane proteins into liposomes. Liposomes B 372:65–86

Rigaud JL, Paternostre MT, Bluzat A (1988) Mechanism of membrane-protein insertion into liposomes during reconstitution procedures involving the use of detergents. 2. Incorporation of the light-driven proton pump bacteriorhodopsin. Biochemistry 27:2677–2688

Rigaud J-L, Pitard B, Levy D (1995) Reconstitution of membrane proteins into liposomes: application to energy-transducing membrane proteins. Biochim Biophys Acta BBA Bioenerg 1231:223–246

Sanat K, Raghunathan VA, Satyajit M (2005) Phase behaviour of dipalmitoyl phosphatidylcholine (DPPC)-cholesterol membranes. J Phys Condens Matter 17:S1177

Sato N (2004) Roles of the acidic lipids sulfoquinovosyl diacylglycerol and phosphatidylglycerol in photosynthesis: their specificity and evolution. J Plant Res 117:495–505

Seddon AM, Curnow P, Booth PJ (2004) Membrane proteins, lipids and detergents: not just a soap opera. Biochim Biophys Acta BBA Biomembr 1666:105–117

Silvius JR (1992) Solubilization and functional reconstitution of biomembrane components. Annu Rev Biophys Biomol Struct 21:323–348

Sokolov VS, Sokolenko EA, Sokolov AV, Dontsov AE, Chizmadzhev YA, Ostrovsky MA (2007) Interaction of pyridinium bis-retinoid (A2E) with bilayer lipid membranes. J Photochem Photobiol B 86:177–185

Sorrenti A, Illa O, Ortuno RM (2013) Amphiphiles in aqueous solution: well beyond a soap bubble. Chem Soc Rev 42:8200–8219

Spassova M, Mellor IR, Petrov AG, Beattie KA, Codd GA, Vais H, Usherwood PNR (1995) Pores formed in lipid bilayers and in native membranes by Nodularin, a cyanobacterial toxin. Eur Biophys J 24:69–76

Stuart MCA, Boekema EJ (2007) Two distinct mechanisms of vesicle-to-micelle and micelle-to-vesicle transition are mediated by the packing parameter of phospholipid–detergent systems. Biochim Biophys Acta BBA Biomembr 1768:2681–2689

Sudbrack TP, Archilha NL, Itri R, Riske KA (2011) Observing the solubilization of lipid bilayers by detergents with optical microscopy of GUVs. J Phys Chem B 115:269–277

Szoka F, Papahadjopoulos D (1980) Comprehensive properties and methods of preparation of lipid vesicles (liposomes). Annu Rev Biophys Bioeng 9:467–508

Yang ZL, Su XH, Wu F, Gong YD, Kuang TY (2005) Photochemical activities of plant photosystem I particles reconstituted into phosphatidylglycerol liposomes. J Photochem Photobiol B Biol 78:125–134

Yasmann A, Sukharev S (2015) Properties of diphytanoyl phospholipids at the air–water interface. Langmuir 31:350–357